

Opportunities for U.S. Contributions to JUNO*

Executive Summary

JUNO provides a rich physics program that complements the existing and planned U.S. neutrino program (Fig. 1) and enhances its physics reach. JUNO will be the first experiment to simultaneously observe neutrino oscillations from both atmospheric and solar neutrino mass-squared splittings and to simultaneously observe more than two oscillation cycles associated with the atmospheric mass-squared splitting. The sub-percent JUNO measurements of oscillation parameters in both the solar ($\sin^2 \theta_{21}$ and Δm_{21}^2) and atmospheric (Δm_{ee}^2) sectors will be invaluable by enabling future sub-percent unitarity tests of the PMNS neutrino mixing matrix and providing valuable input to neutrinoless double beta decay experiments. Precision measurements may also shed light on models explaining neutrino mass and mixing. JUNO's precision measurements in the solar sector cannot be equaled in the foreseeable future before a neutrino factory is built.

In addition, JUNO aims to resolve the neutrino mass hierarchy, aided by precision $\Delta m_{\mu\mu}^2$ measurements from accelerator experiments like T2K and NO ν A. The JUNO mass hierarchy measurement is complementary to that of accelerator experiments such as LBNE or atmospheric experiments such as PINGU in that it does not depend on the 'matter effect'. Combined measurements of this important characteristic of the neutrino mass states with widely varying techniques will enhance confidence in the determination.

Leveraging the very successful U.S-China collaboration on Daya Bay and U.S. experience with a number of neutrino experiments, the U.S. is in a position to play an important role in JUNO. A modest investment at the level of ~\$20M will enable US groups to make key contributions to JUNO centered around the development and fabrication of a calibration system and the precision calibration of the JUNO detector. This investment will allow the U.S. to continue the successful reactor neutrino program into the next generation. JUNO, received 2 billion yuan (~\$300M) funding commitment from the Chinese government, will start construction in 2015 with first physics data in 2020.

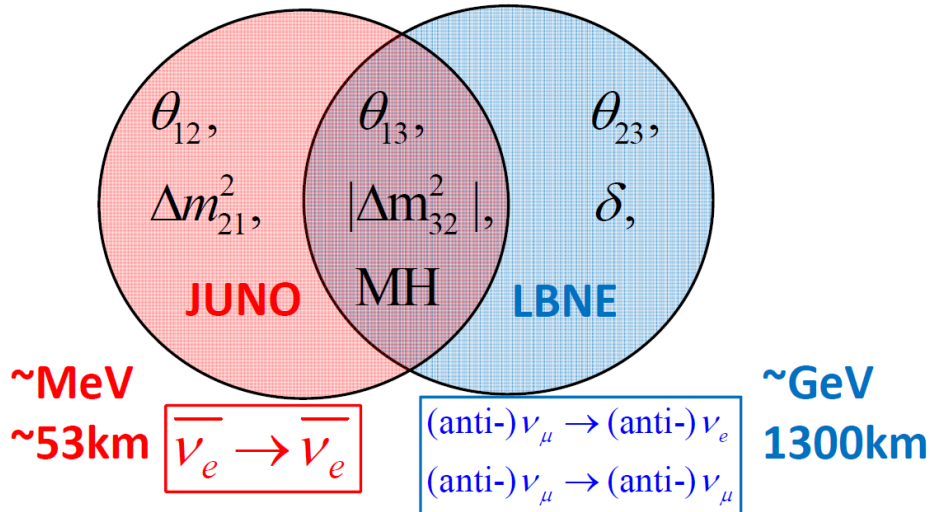


Figure 1: Seven fundamental parameters govern the phenomenon of neutrino oscillation in the standard 3-flavor neutrino framework. JUNO together with LBNE can access all seven parameters.

*Prepared for the Particle Physics Project Prioritization Panel

Opportunities for U.S. Contributions to JUNO

A.B. Balantekin¹³, H. Band^{14,13}, R. Betts⁷, J.J. Cherwinka¹³, J.A. Detwiler¹¹, S. Dye⁵, K.M. Heeger^{14,13},
R. Johnson³, S.H. Kettell¹, T. Langford¹⁴, K. Lau⁶, J.G. Learned⁴, C.J. Lin², J.J. Ling⁸, B. Littlejohn³,
D.W. Liu⁶, K.B. Luk², J. Maricic⁴, K. McDonald⁹, R.D. McKeown¹², J. Napolitano¹⁰, J.C. Peng⁸, X. Qian¹,
N. Tolich¹¹, W. Wang¹², C. White⁷, M. Yeh¹, C. Zhang¹, and T. Zhao¹¹

¹*Brookhaven National Laboratory, Upton, NY, USA*

²*University of California and Lawrence Berkeley National Laboratory, Berkeley, CA, USA*

³*University of Cincinnati, Cincinnati, OH, USA*

⁴*University of Hawaii, Honolulu, HA, USA*

⁵*Hawaii Pacific University, Kaneohe, HA, USA*

⁶*University of Houston, Houston, TX, USA*

⁷*Illinois Institute of Technology, Chicago, IL, USA*

⁸*University of Illinois at Urbana-Champaign, Urbana, IL, USA*

⁹*Princeton University, Princeton, NJ, USA*

¹⁰*Temple University, Philadelphia, PA, USA*

¹¹*University of Washington, Seattle, WA, USA*

¹²*College of William and Mary, Williamsburg, VA, USA*

¹³*University of Wisconsin, Madison, WI, USA*

¹⁴*Yale University, New Haven, CT, USA*

Abstract

The JUNO experiment in southern China will collect 100k inverse beta decay events with a 20 kt liquid-scintillator (LS) detector and ~ 36 GW_{th} reactor power at a baseline of ~ 53 km in six years. Such an enormous neutrino event sample, together with the superior detector energy response and optimal baseline, will allow sub-percent precision measurements of the solar sector and the atmospheric mass-squared splitting. In addition, JUNO aims to resolve the neutrino mass hierarchy. JUNO represents a tremendous scientific opportunity for the U.S. high energy physics community, building on successful U.S.-China collaboration on the Daya Bay experiment. A modest U.S. investment could provide a robust JUNO calibration system and take advantage of existing U.S. expertise in liquid-scintillator technology to ensure the success of JUNO and enable a significant U.S. impact.

1 Introduction

In the standard 3-flavor neutrino framework, there are seven fundamental parameters that describe neutrino oscillations. They include i) three PMNS mixing angles θ_{12} , θ_{23} , and θ_{13} [1, 2, 3], ii) the CP phase δ , iii) atmospheric mass-squared splitting $|\Delta m_{32}^2| := |m_3^2 - m_2^2|$ (or $|\Delta m_{31}^2| := |m_3^2 - m_1^2|$) and solar mass-squared splitting $\Delta m_{21}^2 := m_2^2 - m_1^2$, and iv) the sign of Δm_{32}^2 , which is commonly referred to as the neutrino mass hierarchy (MH).^{*} With $\sim 100\text{k}$ IBD (inverse-beta decay) events from reactor antineutrinos (six years data taking with a 20 kt detector at 36 GW_{th} reactor power), JUNO (Jiangmen Underground Neutrino Observatory) will access five (out of seven) fundamental parameters: θ_{12} , θ_{13} , Δm_{21}^2 , $|\Delta m_{32}^2|$ and MH. These precision neutrino mixing measurements are complementary to measurements from accelerator experiments, such as LBNE [4] that will also access five fundamental parameters: θ_{13} , θ_{23} , δ , $|\Delta m_{32}^2|$ and MH. Figure 1 shows the complementarity between LBNE and JUNO.

JUNO will measure reactor antineutrino disappearance, with the goals of:

- the first experiment to simultaneously observe neutrino oscillations from both atmospheric and solar neutrino mass-squared splittings (Fig. 2).
- the first experiment to observe more than two oscillation cycles of the atmospheric mass-squared splitting (Fig. 2).

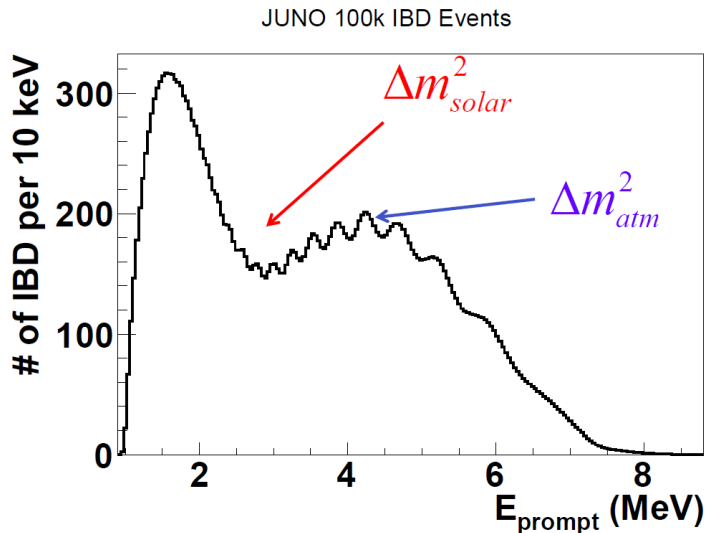


Figure 2: The expected nominal prompt energy spectrum of JUNO. A total of 100k IBD events, which corresponds to six years of data taking with a 20 kt detector and 36 GW_{th} reactor power, is assumed. The big dip around 3 MeV corresponds to the solar oscillation (Δm_{21}^2). The small wiggles from 2 to 8 MeV correspond to the atmospheric oscillation (Δm_{3x}^2). A $3\%/\sqrt{E}$ energy resolution is assumed.

- precision measurements of $\sin^2 2\theta_{21}$, $|\Delta m_{32}^2|$ and Δm_{21}^2 to better than 1%.[†]
- the crown jewel of Reactor $\bar{\nu}_e$: determination of the neutrino MH through measurement of spectral distortion.

^{*}Here, m_1 , m_2 , and m_3 are the masses of the three neutrino mass eigenstates.

[†]The precision measurement of $|\Delta m_{32}^2|$ actually requires knowledge of the MH. In the case of undetermined MH, two results of $|\Delta m_{32}^2|$ would be presented: one for each MH.

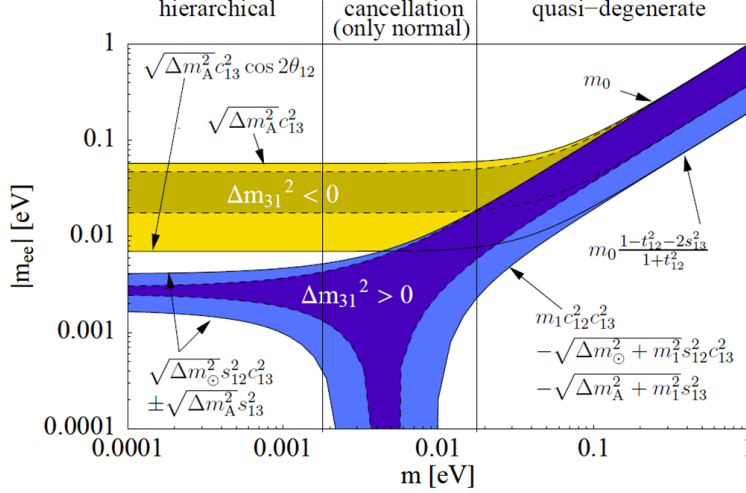


Figure 3: Taken from Ref. [7]. The main properties of the effective mass $|m_{ee}|$ as function of the smallest neutrino mass. Here m_0 denotes the common mass for the quasi-degenerate region and $t_{ij} = \tan \theta_{ij}$, $s_{ij} = \sin \theta_{ij}$, $c_{ij} = \cos \theta_{ij}$. Furthermore, Δm_A^2 and Δm_\odot^2 stands for the atmospheric mass-squared splitting and the solar mass-squared splitting, respectively.

This note is organized as follows: Sec. 2 will focus on the precision JUNO measurement of neutrino mixing parameters. Section 3 will discuss the measurement of the MH. Description of the JUNO project and the potential U.S. contribution can be found in Sec. 4 and Sec. 5, respectively.

2 Precision Measurements of Neutrino Mixing

The precision measurement of neutrino mixings is a very powerful tool to test the standard 3-flavor neutrino model (νSM). In particular, the precision measurement of the fundamental parameter $\sin^2 2\theta_{12}$ will

- lay the foundation for a future sub-1% direct unitarity test of the PMNS matrix U .[‡] The combination of short-baseline reactor antineutrino experiments (such as Daya Bay, RENO and Double Chooz), medium-baseline reactor antineutrino experiments (such as KamLAND and JUNO) and solar neutrino experiments (such as SNO) enable the first direct unitarity test of the PMNS matrix [5, 6]: $|U_{e1}|^2 + |U_{e2}|^2 + |U_{e3}|^2 \stackrel{?}{=} 1$. When combined with Daya Bay and SNO, JUNO's precision measurement will test this unitarity condition to 2.5% [6]. The precision is limited by the solar neutrino measurements and could be improved to better than 1% with future precision solar neutrino measurements.
- constrain the allowed region of the effective neutrino mass $|m_{ee}| := |\sum U_{ei}^2 m_i|$, to which the decay width of neutrinoless double beta decay is proportional. Figure 3 shows the dependence of $|m_{ee}|$ on the smallest neutrino mass m_1 for both normal and inverted mass hierarchies. In the region where the smallest neutrino mass is smaller than 0.002 eV, the θ_{12} angle directly affects the lower bound of $|m_{ee}|$ for the inverted mass hierarchy that is the goal of the next-generation neutrinoless double beta decay experiments.[§]

[‡]The unitarity condition refers to $U \times U^+ = I$ and $U^+ \times U = I$, in which I is the 3×3 unit matrix.

[§]We note that the nuclear matrix element will be one of the major uncertainties in deducing constraints of $|m_{ee}|$ from the neutrinoless double beta decay experiments.

- test models of neutrino masses and mixings. As summarized in the Ref. [8], various models predict sum rules connecting neutrino mixing parameters, such as $\theta_{12} = 35^\circ + \theta_{13} \cos \delta$, $\theta_{12} = 32^\circ + \theta_{13} \cos \delta$, and $\theta_{12} = 45 + \theta_{13} \cos \delta$. Testing these sum rules will shed light on the questions of why the leptonic mixing angles are large compared to the quark CKM mixing angles and whether there is any pattern hidden in the leptonic mixing angles that could guide us towards a more complete theory of flavor [9].

As shown in Ref. [10], the measurements of muon (anti)neutrino disappearance and electron antineutrino disappearance are effectively measuring $\Delta m_{\mu\mu}^2$ and Δm_{ee}^2 (two different combinations of Δm_{31}^2 and Δm_{32}^2), respectively. When combined with the precision $|\Delta m_{\mu\mu}^2|$ measurements from muon (anti)neutrino disappearance, the precision measurement of $|\Delta m_{ee}^2|$ will

- test the sum rule $\Delta m_{13}^2 + \Delta m_{21}^2 + \Delta m_{32}^2 = 0$, which is an important prediction of the νSM .
- reveal additional information regarding the neutrino mass hierarchy. Using the convention of Ref. [11], we have $|\Delta m_{ee,\mu\mu}^2| \approx |\Delta m_{23}^2| \pm \Delta m_\phi^2_{ee,\mu\mu}/2$, in which the plus/minus sign depends on the mass hierarchy. Since the $\Delta m_\phi^2_{ee}$ ($\sim 10^{-4} eV^2$) are larger than $\Delta m_\phi^2_{\mu\mu}$ ($\sim 5 \times 10^{-5} eV^2$), the precision measurements of both $|\Delta m_{\mu\mu}^2|$ and $|\Delta m_{ee}^2|$ would provide new information regarding the neutrino mass hierarchy.

JUNO will measure the solar oscillation parameters: $\sin^2 2\theta_{12}$ and Δm_{21}^2 , and the atmospheric oscillation parameter $|\Delta m_{32}^2|$ to better than 1% with the disappearance of reactor electron antineutrinos. More specifically, as shown in Ref. [12], the expected precision of Δm_{21}^2 , Δm_{32}^2 , and $\sin^2 2\theta_{21}$ are 0.3%, 0.3%, and 0.6%, respectively. Recently, we carried out an independent analysis [13] of the JUNO sensitivity based on tools developed in the Daya Bay rate+shape analysis [14]. The systematic uncertainties implemented in our study include: i) accidental backgrounds, ${}^9\text{Li}/{}^8\text{He}$ backgrounds, fast neutron backgrounds, $\alpha\text{-N}$ backgrounds, and geo-neutrino backgrounds, which are scaled from KamLAND or Daya Bay. ii) constraint of reactor spectrum [15, 16], iii) absolute energy model, and iv) absolute normalization. Our results are consistent with those from Ref. [12]. In particular, we found that at $3\%/\sqrt{E}$ energy resolution and 1% energy uncertainty with a Daya Bay style energy model [14], the expected precision of Δm_{21}^2 , Δm_{32}^2 , and $\sin^2 2\theta_{21}$ are 0.4%, 0.3%, and 0.5%, respectively. We further studied the impact of the energy resolution: Δm_{21}^2 and $\sin^2 2\theta_{21}$ have very weak dependencies on the energy resolution, while the precision Δm_{32}^2 degraded slightly with worse energy resolution (0.3% at $3\%/\sqrt{E}$ to 0.6% at $6\%/\sqrt{E}$). Our study showed that the precision JUNO measurement of neutrino mixing parameters is robust.

3 The Crown Jewel of Reactor $\bar{\nu}_e$: the Neutrino Mass Hierarchy

Neutrino mass hierarchy, whether the third generation neutrino mass eigenstate is heavier or lighter than the first two, is one of the three remaining unknowns in the νSM .[¶] The determination of the neutrino mass hierarchy together with searches for neutrinoless double beta-decay may reveal whether neutrinos are Dirac or Majorana fermions, which could significantly advance our understanding of the universe.

The precise measurement of $\sin^2 2\theta_{13}$ by the current generation of short-baseline reactor neutrino experiments [17, 18, 19] has provided a unique opportunity to determine the MH in a medium baseline (~ 55 km) reactor neutrino experiment [20, 21, 22, 23, 11, 24, 25, 26]. The oscillation from the atmospheric mass-squared splitting manifests itself in the energy spectrum as multiple cycles which

[¶]The other two unknowns are CP phase δ and the absolute neutrino mass.

contain the MH information, as shown in the following formula,

$$\begin{aligned}
P_{\bar{\nu}_e \rightarrow \bar{\nu}_e} &= 1 - \sin^2 2\theta_{13}(\cos^2 \theta_{12} \sin^2 \Delta_{31} + \sin^2 \theta_{12} \sin^2 \Delta_{32}) - \cos^4 \theta_{13} \sin^2 2\theta_{12} \sin^2 \Delta_{21} \\
&= 1 - 2s_{13}^2 c_{13}^2 - 4c_{13}^2 s_{12}^2 c_{12}^2 \sin^2 \Delta_{21} + 2s_{13}^2 c_{13}^2 \sqrt{1 - 4s_{12}^2 c_{12}^2 \sin^2 \Delta_{21} \cos(2\Delta_{32} \pm \phi)},
\end{aligned} \tag{1}$$

where $\Delta_{21} \equiv \Delta m_{21}^2 L/4E$, $\Delta_{32} \equiv \Delta m_{32}^2 L/4E$, in which L is the baseline and E is the antineutrino energy, and

$$\sin \phi = \frac{c_{12}^2 \sin 2\Delta_{21}}{\sqrt{1 - 4s_{12}^2 c_{12}^2 \sin^2 \Delta_{21}}}, \quad \cos \phi = \frac{c_{12}^2 \cos 2\Delta_{21} + s_{12}^2}{\sqrt{1 - 4s_{12}^2 c_{12}^2 \sin^2 \Delta_{21}}}.$$

The \pm sign in last term of Eq. (1) is decided by the MH: plus sign for NH and minus sign for IH. The principle of the MH determination through spectral distortion can be easily understood from the left panel of Fig. 4 that shows the energy and baseline dependent $\Delta m_\phi^2 := 4E\phi/L$ based on Eq. 1.

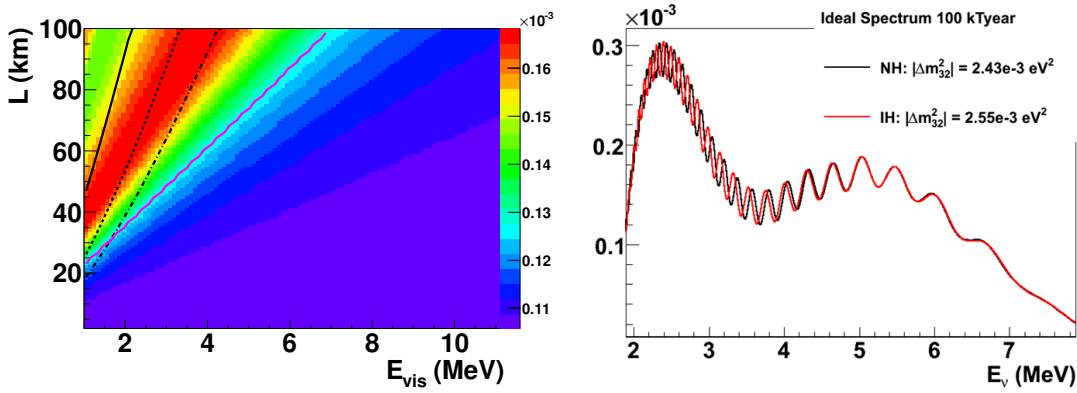


Figure 4: Left: Taken from Ref. [11]. The effective mass-squared difference shift Δm_ϕ^2 as a function of baseline and visible prompt energy $E_{vis} \approx E_\nu - 0.8 \text{ MeV}$. Right: the ideal spectral distortion at JUNO for both normal and inverted hierarchies with perfect energy resolution.

At $\sim 55 \text{ km}$ baseline, the Δm_ϕ^2 at low energy ($\sim 3 \text{ MeV}$) is larger than the Δm_ϕ^2 at high energy ($\sim 6 \text{ MeV}$). For NH, the effective atmospheric mass-squared difference $\Delta m_{ee}^2 = 2\Delta m_{32}^2 + \Delta m_\phi^2$ at low energy will be larger than that at high energy and vice versa for IH, in which the effective mass-squared difference is $\Delta m_{ee}^2 = 2\Delta m_{32}^2 - \Delta m_\phi^2$. The difference in the spectral distortion (ideal with perfect energy resolution) for NH and IH is shown in the right panel of Fig. 4.

JUNO plans to resolve the MH. The requirements are:

- **Better than $\sim 3\%/\sqrt{E(\text{MeV})}$ energy resolution.** Determination of the MH requires measurements of the effective mass-squared splitting at both high and low energy. At low energy, due to the long baseline, the L/E value is quite large. Therefore, a sizable energy resolution would smear the oscillation cycles, impeding the measurement of Δm_{ee}^2 . Reference [21, 27, 22, 23, 11] show that energy resolution better than $\sim 3\%/\sqrt{E(\text{MeV})}$ is needed in order to resolve the difference between NH and IH. To achieve this energy resolution a dedicated R&D program is underway to address the following items [28, 29]:

- high detector photo-cathode coverage $\sim 80\%$,
- high PMT collection and quantum efficiency (QE $\sim 35\%$),
- highly transparent LS with attenuation length of $>30 \text{ m}$ (comparable to the dimension of the 20 kt LS detector),

- high light yield LS ($\sim 1.5\times$ photon yield of KamLAND LS),
 - a comprehensive calibration system which controls the smearing due to position-dependent energy response across the detector.
- **A suitable site relative to the reactor cores.** The key for JUNO to resolve MH and to reach high precision in Δm_{ee}^2 is to clearly observe multiple oscillation cycles from the atmospheric mass-squared splitting. For the peak reactor antineutrino energy, the corresponding oscillation length is ~ 2 km. Therefore, if the baseline difference is ~ 2 km in a two-reactor configuration, the oscillation signal corresponding to the atmospheric mass squared splitting will be strongly suppressed. More specifically, Ref. [26] showed that the MH sensitivity is largely reduced if the baseline difference is around 1.5 km for the two-reactor configuration.
 - **A high statistics IBD sample ($\sim 100\text{k}$) is required.** At $\sim 3\%/\sqrt{E(\text{MeV})}$ energy resolution, the effect of MH in the spectral distortion is modest. It is important to collect a total of $\sim 100\text{k}$ IBD events in JUNO, which can be achieved with a 20 kt LS detector at ~ 53 km baseline together with a total of 36 GW_{th} reactor power in 5–6 (calendar) years of data taking.
 - **A $< 1\%$ absolute energy scale uncertainty [11, 13].** Since the MH information is embedded in the spectral distortion, it is important to control the uncertainty in the energy model that connects the reconstructed positron energy spectrum to the neutrino spectrum. Development of a sophisticated calibration system is essential to achieve this goal.

In the following we illustrate JUNO’s sensitivity to the MH. Given a measurement, we would compare the data x with expectations from both NH and IH hypotheses. In practice, one commonly defines a test statistics $T_{NH} := -2\text{Log}(L_{NH})$, where L_{NH} is the likelihood of NH for data x . T_{NH} is further minimized over all nuisance parameters to obtain T_{NH}^{min} . Similarly, T_{IH}^{min} is calculated from the likelihood of IH for data x . In order to evaluate whether the experimental data favors NH or IH, a test statistics $\Delta T = T_{IH}^{min} - T_{NH}^{min}$ is defined. It is easy to see that a positive ΔT would favor the NH, and vice versa. In addition, the absolute size of ΔT indicates how much the data favor one hypothesis relative to the other.

Regarding the JUNO MH sensitivity, we report the average expectation $\overline{\Delta T}$, which is calculated with the Asimov data set.^{||} In addition, as shown in the left panel of Fig. 5, we show the 68% and 95% expectation bands together with the $\overline{\Delta T}$ curve.

The dotted lines correspond to the probability ratios of NH vs. IH in the Bayesian framework [30]. Furthermore, given the observed data ΔT , there is a maximum p-value of the null hypothesis being the disfavored MH hypothesis, which corresponds to $\sqrt{|\Delta T|}$ in terms of number of standard deviations. This sensitivity study is based on calculations from Ref. [26], which assumed a 20 kt detector at ~ 53 km with 36 GW_{th} reactor power. The energy resolution was assumed to be $3\%/\sqrt{E}$. We should point out that JUNO’s MH sensitivity comes from two different types of information. The first type is measured within the experiment itself: the contrast of the atmospheric phase shifts in each oscillation cycle at low and high energy parts of the survival spectrum. The blue curve in the left panel of Fig. 5 represents this first sensitivity. The other type of information lies in the comparison of Δm_{ee}^2 by JUNO and $\Delta m_{\mu\mu}^2$ by superbeam experiments. The red curve in the left panel of Fig. 5 includes the second type contribution with the $\Delta m_{\mu\mu}^2$ assuming to be measured to 1%. Combining the two types of information, JUNO has a robust path to resolve the neutrino mass hierarchy.

^{||}Asimov data set does not include any statistical fluctuation and any variations in systematics.

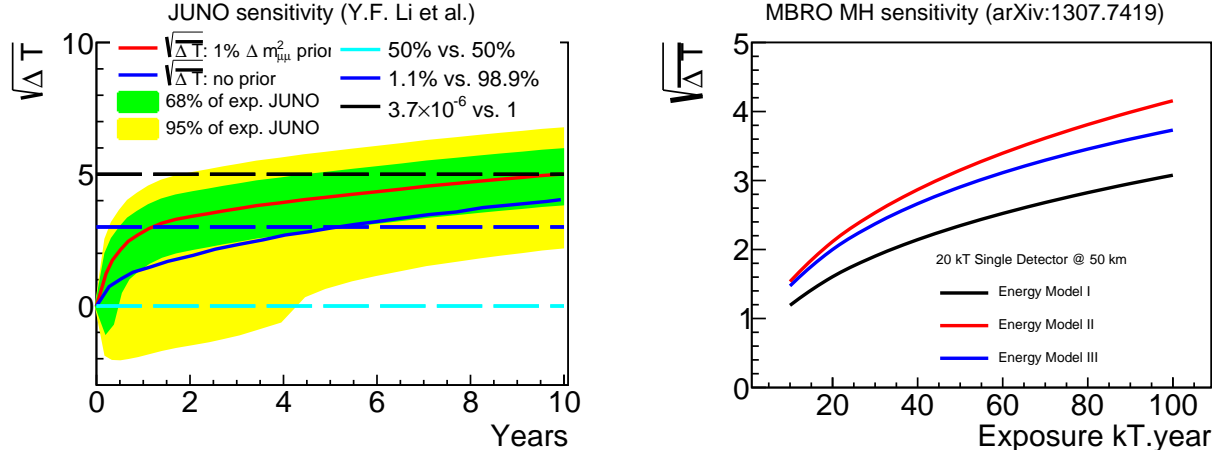


Figure 5: Left: JUNO’s sensitivity calculation based on Ref. [26]. A 20 kt detector at ~ 53 km with a total of 36 GW_{th} reactor power was assumed. The energy resolution was assumed to be $3\%/\sqrt{E}$. Right: MBRO’s (medium baseline reactor experiment) sensitivity calculation based on Ref. [13]. A total of 40 GW_{th} reactor power was assumed. The energy resolution was assumed to be $\sqrt{(0.7\%)^2 + \frac{(2.6\%)^2}{E} + \frac{(0.85\%)^2}{E^2}}$.

The right panel of Fig. 5 shows the results (first type MH sensitivity only) from an independent study of the MH sensitivity in a medium baseline reactor experiment (MBRO) [13]. A 20 kt detector at ~ 50 km with 40 GW_{th} reactor power was assumed. The energy resolution was assumed to be $\sqrt{(0.7\%)^2 + \frac{(2.6\%)^2}{E} + \frac{(0.85\%)^2}{E^2}}$. Furthermore, three different absolute energy models were compared: i) model motivated by Ref. [11] which was designed to reduce the MH sensitivity, ii) 1% uncertainty in the absolute energy scale (linear shift), and iii) based on the Daya Bay energy model [14]. For model I and III, the uncertainty in the absolute energy scale was about 1%. As shown in the right panel of Fig. 5, the MH sensitivity depends on the functional form of the energy model. Therefore, a good energy calibration constraining the absolute scale as well as the functional form of the energy model will increase the MH sensitivity of JUNO.

The neutrino mass hierarchy, likely the next fundamental parameter determined in the standard model, is also one of main goals of LBNE [4] and PINGU [31]. Unlike the JUNO spectral distortion method, the MH determination in LBNE and PINGU depends on the matter effect in the (anti) ν_e appearance with accelerator (anti) ν_μ neutrinos and atmospheric neutrinos oscillations, respectively. These complementary approaches with different techniques are necessary to ensure the MH determination with high confidence.

4 Jiangmen Underground Neutrino Observatory

JUNO is a next-generation (medium-baseline) reactor oscillation experiment that will be built in Jiangmen City, Guangdong Province, China [28, 29, 32]. It consists a 20 kt underground liquid scintillator detector with a 1,850 m water equivalent overburden, and two reactor complexes at baselines of ~ 53 km with a total thermal power of 36 GW (see Fig. 6). It has received 2 billion yuan (\sim \$300M) funding commitment from the Chinese government with a construction starting in 2015 and data taking in 2020. Besides the sub-percent precision measurements of solar sector oscillation parameters and atmospheric mass-squared splitting [26, 13] and the MH determination, the 20 kt target mass offers a rich physics program of proton decay, geoneutrinos, supernova neutrino, and many exotic neutrino



Figure 6: Conceptual design of the JUNO detector. Various options of realizing the design are under review including this one. The major differences lie in the mechanism of separating the LS and MO volumes. Three options are under consideration: an acrylic sphere like SNO (shown), a nylon balloon like BOREXINO and KamLAND and encapsulated PMTs in acrylic modules filled with MO.

physics topics [13]. It is worth noting that in the $p \rightarrow \nu + K^+$ channel, JUNO could be competitive with other running and to-be-built experiments like Super-K, LBNE, and Hyper-K [13].

Figure 6 shows the conceptual design of JUNO’s 20 kt LS detector [33, 34]. A spherical LS target volume is chosen to minimize the surface-to-volume ratio and PMT cost. This will also minimize position dependent corrections to the reconstructed energy, which is crucial for the MH determination as illustrated in Sec. 3. The design shown in Fig. 6 is one of the three major options that JUNO is considering: acrylic sphere, balloon and acrylic modules. The major design differences regard the separation of the MO and LS volumes [33, 34]. To achieve the desired $3\%/\sqrt{E}$ energy resolution, JUNO has initiated an extensive R&D program:

- Increase photo-cathode coverage to $\sim 80\%$ [34]. Compared with $\sim 40\%$ in the Super-K water Cerenkov detector and $\sim 34\%$ in the BOREXINO and KamLAND LS detectors, the proposed coverage will be the highest ever. It has been shown that $\sim 74\text{--}83\%$ photo-cathode coverage can be achieved by careful consideration of PMT protection.
- Increase LS photon yield and LS attenuation length. High performance LS with high intrinsic photon yield (>14000 photons per MeV) and superior optical attenuation length of 30 m or better is crucial to reach the required energy resolution for MH determination in JUNO. Extensive LS studies are ongoing and U.S. expertise is well matched to this critical R&D. The LS attenuation length could be increased by removing the light absorbing molecules. Currently, it has been demonstrated that transparency length ~ 24 m is possible [35]. On-going efforts are aiming to reach >30 m attenuation length.
- Increase PMT quantum efficiency. Currently, JUNO has two proposals to increase PMT quantum efficiency. One solution is the commercially available super-bialkali Hamamatsu PMT. Another option is to develop a new type of high quantum efficiency microchannel-plate (MCP) based PMT [36]. MCP PMT prototypes have been produced and single photo-electron peaks have been successfully observed with satisfactory PMT gains. More studies are needed to reach the desired quantum efficiency [36].

Figure 7 shows the layout of the experiment that includes both the nuclear reactor complexes (Taishan and Yangjiang reactor cores) and the JUNO detector. The detector location, under a small



Figure 7: The JUNO site in southern China. For comparison, the previously considered site near Daya Bay is also shown. The Daya Bay site has more complicated reactor baselines and is not suitable for JUNO. These reactors are over 200 km away from the current site thus have little impact on JUNO.

mountain near Kaiping City, is optimized to maximize the MH sensitivity. A geological survey has been performed and the rock structure and quantity are suitable for underground lab construction [32]. Table 1 summarizes the JUNO baselines. All cores are either running or under construction except

Table 1: JUNO reactor power and baseline combinations. Taishan Core III and IV have been approved for construction. However, the construction date is not fixed at the time this document is prepared.

Cores	YJI	YJII	YJIII	YJIV	YJV	YJVI	TSI	TSII	TSIII	TSIV
Power (GW_{th})	2.9	2.9	2.9	2.9	2.9	2.9	4.6	4.6	4.6	4.6
Baseline(km)	52.75	52.84	52.42	52.51	52.12	52.21	52.76	52.63	52.32	52.20

the 3rd and 4th cores of the Taishan nuclear power plant, which are approved for construction. At the time this document is prepared, the construction date is not fixed for the latter two cores. The combination of baselines, with a mean of 52.48 km and RMS (root mean square) 0.25 km, will allow a determination of MH. The impact of different baselines has been taken into account in the MH sensitivity study of Ref. [26] (left panel of Fig. 5).

5 Scope of Potential U.S. Contributions

The U.S. MBRO (medium baseline reactor experiment) working group [13] has an established record in the energy calibration of the SNO (D_2O) [37], KamLAND (LS) [38], Super-Kamiokande (H_2O) [39, 40], and Daya Bay (LS) [41] detectors and has thoroughly studied the energy scale requirements to meet the physics goals of JUNO [11, 13]. U.S. expertise is well matched to the design & construction of the JUNO calibration system. The success of the calibration program will determine whether JUNO will be able to determine the mass hierarchy.

5.1 A Comprehensive Approach to the Calibration of JUNO

The liquid scintillator energy scale from 0.5-10 MeV is not linear due to scintillation quenching, Cherenkov light emission, readout electronics effects and positional variation of detector energy response. Precise understanding of the energy response of a large LS detector requires a comprehensive calibration program to:

- determine the detector response to various particle types (β , e^+ , neutrons and γ),
- evaluate the energy response throughout the detector volume,
- calibrate event reconstruction to determine the fiducial volume,
- monitor stability of the energy response.

KamLAND, Double Chooz, and Daya Bay have utilized a variety of calibration systems designed to address the routine calibration and monitoring needs of these experiments as well as the characterization of the entire detector volume. The size of the JUNO detector poses significant challenges to the realization of a full-volume calibration program over the energy range of the reactor antineutrino spectrum. Specific challenges in the context of the JUNO detector include:

- the deployment of point-like calibration sources throughout the detector volume,
- the number of calibration source positions that can be sampled in a reasonable time,
- the understanding of the integrated detector response.

The calibration requirements of JUNO combined with its size demand novel and innovative approaches to detector calibration. As part of the planned calibration program for JUNO we consider mono-energetic radioactive sources as well as man-made variable energy sources, point-like sources and uniformly distributed sources, as well as short-lived positron emitters.

The deliverables of a US-led effort on the JUNO calibration program will include:

1. design and fabrication of a comprehensive suite of calibration sources,
2. development and implementation of a precise positioning system for radioactive and light sources throughout the 20 kt detector,
3. development of a production system for short-lived radioactive isotopes to calibrate the detector volume with uniformly distributed sources,
4. development and integration of a variable energy accelerator for the calibration of the reactor antineutrino spectrum region of interest.

5.2 Radioactive Calibration Sources

The detection of antineutrinos with a large liquid scintillator detector requires calibration of the detector response to e^+ , β , γ and neutrons over the energy range 0.5-10 MeV. The energy range of interest is determined by the reactor spectrum.

Radioactive sources of well-defined energy can establish low-energy detector response to gammas. Typical sources are ^{137}Cs (0.661 MeV), ^{54}Mn (0.835 MeV), ^{68}Ge (2×0.511 MeV), ^{22}Na (1.274 MeV), ^{60}Co (1.332 MeV), and ^{40}K (1.460 MeV). Neutron calibration sources include ^{241}Am - ^{13}C , ^{252}Cf or Am-Be. Stable and pulsed LED sources as well as light sources based on scintillator sources (e.g. ^{137}Cs) will be used for PMT calibration. The source rate and specific geometric design (including encapsulation) will be optimized with GEANT4 simulations. Prototype sources will be procured, fabricated and characterized to meet the calibration time requirements. Gamma sources are easy to obtain and encapsulate but their energies are limited to <3 MeV. Higher-energy calibrations require other approaches.

Short-lived isotopes offer an opportunity for calibration with well-known beta spectra, with higher-energy gamma rays that are otherwise inaccessible or with distributed sources throughout the detector

volume. Short-lived sources were successfully deployed in SNO to simulate the ^8B neutrino spectrum. Two examples of artificially produced short-lived calibration sources are ^{16}N [42] and ^8Li [43]. The ^8Li isotope can be created with a commercial deuterium-tritium (DT) neutron generator through the $^{11}\text{B}(n,\alpha)$ reaction and it decays with a Q-value of ~ 16.0 MeV. The main beta-decay branch has an end-point energy of 12.96 MeV. The ^8Li isotope can be carried several meters to a decay chamber suspended inside the detector using a gas/aerosol transport system as in SNO. The ^{16}N isotope can be produced via the $^{16}\text{O}(n,p)$ reaction in CO_2 gas. A gas stream in capillary tubing can transfer the isotope into a decay chamber. In the case of SNO, the decay and trigger chamber blocked energetic beta-particles but permitted the 6.13 MeV gamma-ray to enter the detector. The ~ 6 MeV gamma ray was the primary energy calibration in SNO as well as verification of the energy resolution and energy scale position dependence. We will study the use of these sources for a 20 kt liquid scintillator detector and develop a transfer and injection system. The transfer of the isotopes over the longer distances in a 20 kt liquid scintillator detector will pose new challenges.

Calibration of the entire volume of a large liquid scintillator detector can only be achieved with distributed sources in the scintillator. Detector calibration with uniformly distributed sources allows calibration of the integrated detector response and comparison of events of known energies in different regions of the detector. At SNO ^{24}Na and ^{222}Rn were successfully used for in-situ detector calibration. In particular, the alpha sources could provide strong constraints on the energy quenching of the LS. Deployment of a variety of positron sources with energies in the non-linear range would provide a more direct indication of the energy scale for the reactor antineutrino signal. Most positron isotopes have short half-lives (from minutes to hours) such that loading them into scintillator would be a challenge. For the calibration of JUNO we will survey short-lived isotopes and study their production and injection concepts with a gas or scintillator stream into the detector. Furthermore, background events (such as ^{12}B beta decay spectrum and ^{208}Tl with 2.614 MeV gamma) provide additional handles in the energy calibration towards high energy.

5.3 Variable Energy Calibration Devices

Precise calibration of the full energy spectrum would benefit from a calibration device with variable energy that allows a scan of the energy region of interest (e.g. visible energy from 1 MeV to 4-6 MeV). We studied various options. The first option is a positron pelletron which will be able to deliver mono-energetic positrons that cover the IBD spectrum continuously from low to high energy. Its dimension is on the order of ~ 10 m and thus can fit in the JUNO experimental hall. Based on a survey of existing facilities, 0.5 to 6.5 MeV (kinetic energy) positron beams can be produced with an accuracy of $\Delta E/E \leq 10^{-4}$ by monitoring the beam energy with a high purity Germanium (HPGe) detector and providing feedback in real time [44]. The pelletron can also switch to use electron sources and provide electron beams in the same energy range. The second option is the low-energy electron accelerators that have broad commercial applications in materials science, gas and water purification, sterilization and cargo inspection. Customized turnkey electron and ion linacs are widely used in research [45, 46]. In the energy range up to 5 MeV direct current accelerators are used. Between 5-10 MeV betatrons or RF linacs are favored. At these low energies no residual radioactivity is created. Direct current accelerators are offered by a number of commercial companies such as the National Electrostatics Corporation [47] in the U.S., the Nissin High Voltage Corporation in Japan [48], and customized turnkey systems for research are offered by Research Instruments GmbH [49] in Germany. Specific challenges include the stability of the beam energy for linacs and the beam delivery into the detector.

With both calibration sources and variable energy devices, we believe a highly accurate energy response model can be obtained to meet the needs of the MH determination.

5.4 Calibration Source Deployment Systems

Injection and deployment of sources in a 35 m-detector poses challenges including i) production and injection of isotopes over long distances, ii) isotope distribution and mixing in the detector, and iii) injection of electron/positron beams into the detector. Deployment systems such as articulated arms used in Daya Bay [50], Double Chooz, and KamLAND [38] are not feasible. Two approaches are under consideration: i) a series of fixed ports which can either load sources or inject electron/positron beam into the detector vertically, ii) a tubular system that can be used to deliver short-lived isotopes into different detector regions, iii) a cable & pulley system such as the one used in SNO [42].

Precise positioning of calibration sources throughout the target volume is important for assessing energy response non-uniformity within the detector. In case of JUNO this will be challenging due to the size of the 20 kt detector. Rapid development of high quality, affordable cameras in recent years provides an attractive option for detector calibration with sources, using cameras to locate the source. Such an approach has been used in Borexino and led to 2 cm positioning precision using a system of cameras mounted on the detector walls. A system of cameras mounted on the walls of the large scintillator detector may potentially allow locating mobile sources to 1 cm. Utilization of such a system would not only provide knowledge of the precise source location, but would simplify the design of the 3D calibration system. Such a 3D positioning system would be free of the need for high precision remote operation and would be much easier and cheaper to fabricate than a mechanical system.

5.5 Additional Efforts

Besides the leading effort in the JUNO calibration system, the U.S. team has also expertise and interest in the following systems for the JUNO experiment:

- Develop high performance liquid scintillator with high intrinsic light yield (>14000 photons per MeV) and good optical transmission (attenuation length of 30 m or better).
- Improve PMT collection efficiency, magnetic field shielding, and mechanical performance. Winston cones could be an attractive option to collect light lost in the spaces between PMTs, which effectively increase the collection efficiency of PMT. For JUNO, a 20 kt detector with over 80% photocoverage, the PMT mechanical performance, especially the survival of an assembled PMT array under significant hydrostatic pressure and subjected to shock waves caused by the failure of a single PMT, needs to be carefully examined.
- Develop techniques for front-end and trigger electronics including the linearity of the charge measurement, dynamic range of time and charge measurements, multiple hit and pileup resolution capability, waveform digitization frequency, types of triggers.

6 Conclusion

A modest U.S. investment in JUNO will leverage the previous collaboration on Daya Bay to ensure success of the international JUNO experiment. As a complementary experiment to LBNE, JUNO will precisely measure the solar oscillation (and atmospheric mass-splitting) parameters and aim for the determination of the mass hierarchy.

A contribution at a level of $\sim\$20\text{M}$ will ensure a critical U.S. role in JUNO and enable key experimental contributions such as the development and fabrication of a calibration system, development and characterization of scintillator and leading the design of the readout electronics. Participation in JUNO will allow the U.S. to continue its successful role in reactor neutrino physics and be a key international collaborator in the next-generation precision reactor oscillation measurements.

References

- [1] B. Pontecorvo, “Mesonium and anti-mesonium,” *Sov.Phys.JETP* **6** (1957) 429.
- [2] B. Pontecorvo, “Neutrino Experiments and the Problem of Conservation of Leptonic Charge,” *Sov.Phys.JETP* **26** (1968) 984–988.
- [3] Z. Maki, M. Nakagawa, and S. Sakata, “Remarks on the unified model of elementary particles,” *Prog.Theor.Phys.* **28** (1962) 870–880.
- [4] **LBNE** Collaboration, C. Adams *et al.*, “Scientific Opportunities with the Long-Baseline Neutrino Experiment,” [arXiv:1307.7335](#) [[hep-ex](#)].
- [5] S. Antusch, C. Biggio, E. Fernandez-Martinez, M. Gavela, and J. Lopez-Pavon, “Unitarity of the Leptonic Mixing Matrix,” *JHEP* **0610** (2006) 084, [arXiv:hep-ph/0607020](#) [[hep-ph](#)].
- [6] X. Qian, C. Zhang, M. Diwan, and P. Vogel, “Unitarity Tests of the Neutrino Mixing Matrix,” [arXiv:1308.5700](#) [[hep-ex](#)].
- [7] W. Rodejohann, “Neutrinoless double beta decay and neutrino physics,” *J.Phys.* **G39** (2012) 124008, [arXiv:1206.2560](#) [[hep-ph](#)].
- [8] **Intensity Frontier Neutrino Working Group** Collaboration, A. de Gouvea *et al.*, “Neutrinos,” [arXiv:1310.4340](#) [[hep-ex](#)].
- [9] S. Antusch, “Models for Neutrino Masses and Mixings,” *Nucl.Phys.Proc.Suppl.* **235-236** (2013) 303–309, [arXiv:1301.5511](#) [[hep-ph](#)].
- [10] H. Nunokawa, S. J. Parke, and R. Zukanovich Funchal, “Another possible way to determine the neutrino mass hierarchy,” *Phys.Rev.* **D72** (2005) 013009, [arXiv:hep-ph/0503283](#) [[hep-ph](#)].
- [11] X. Qian, D. Dwyer, R. McKeown, P. Vogel, W. Wang, *et al.*, “Mass Hierarchy Resolution in Reactor Anti-neutrino Experiments: Parameter Degeneracies and Detector Energy Response,” *PRD*, *87*, **033005** (2013), [arXiv:1208.1551](#) [[physics.ins-det](#)].
- [12] J. Cao, “Daya bay-ii: A 60 km-baseline reactor experiment and beyond,” in *International Symposium on Neutrino Physics and Beyond*. 2012.
- [13] A. B. Balantekin *et al.*, “Neutrino mass hierarchy determination and other physics potential of medium-baseline reactor neutrino oscillation experiments,” [arXiv:1307.7419](#) [[hep-ex](#)].
- [14] **Daya Bay** Collaboration, F. An *et al.*, “Spectral measurement of electron antineutrino oscillation amplitude and frequency at Daya Bay,” [arXiv:1310.6732](#) [[hep-ex](#)].
- [15] P. Huber, “On the determination of anti-neutrino spectra from nuclear reactors,” *Phys.Rev.* **C84** (2011) 024617, [arXiv:1106.0687](#) [[hep-ph](#)].
- [16] T. Mueller, D. Lhuillier, M. Fallot, A. Letourneau, S. Cormon, *et al.*, “Improved Predictions of Reactor Antineutrino Spectra,” *Phys.Rev.* **C83** (2011) 054615, [arXiv:1101.2663](#) [[hep-ex](#)].
- [17] **Daya Bay** Collaboration, F. An *et al.*, “Observation of electron-antineutrino disappearance at Daya Bay,” *Phys.Rev.Lett.* **108** (2012) 171803, [arXiv:1203.1669](#) [[hep-ex](#)].
- [18] **Daya Bay** Collaboration, F. An *et al.*, “Improved Measurement of Electron Antineutrino Disappearance at Daya Bay,” *Chin. Phys.* **C37** (2013) 011001, [arXiv:1210.6327](#) [[hep-ex](#)].

- [19] **RENO** Collaboration, J. Ahn *et al.*, “Observation of Reactor Electron Antineutrino Disappearance in the RENO Experiment,” *Phys.Rev.Lett.* **108** (2012) 191802, [arXiv:1204.0626 \[hep-ex\]](#).
- [20] S. Petcov and M. Piai, “The LMA MSW solution of the solar neutrino problem, inverted neutrino mass hierarchy and reactor neutrino experiments,” *Phys.Lett.* **B533** (2002) 94–106, [arXiv:hep-ph/0112074 \[hep-ph\]](#).
- [21] J. Learned, S. T. Dye, S. Pakvasa, and R. C. Svoboda, “Determination of neutrino mass hierarchy and θ_{13} with a remote detector of reactor antineutrinos,” *Phys.Rev.* **D78** (2008) 071302, [arXiv:hep-ex/0612022 \[hep-ex\]](#).
- [22] L. Zhan, Y. Wang, J. Cao, and L. Wen, “Determination of the Neutrino Mass Hierarchy at an Intermediate Baseline,” *Phys.Rev.* **D78** (2008) 111103, [arXiv:0807.3203 \[hep-ex\]](#).
- [23] L. Zhan, Y. Wang, J. Cao, and L. Wen, “Experimental Requirements to Determine the Neutrino Mass Hierarchy Using Reactor Neutrinos,” *Phys.Rev.* **D79** (2009) 073007, [arXiv:0901.2976 \[hep-ex\]](#).
- [24] E. Ciuffoli, J. Evslin, and X. Zhang, “The Neutrino Mass Hierarchy at Reactor Experiments now that θ_{13} is Large,” *JHEP* **1303** (2013) 016, [arXiv:1208.1991 \[hep-ex\]](#).
- [25] S.-F. Ge, K. Hagiwara, N. Okamura, and Y. Takaesu, “Determination of mass hierarchy with medium baseline reactor neutrino experiments,” *JHEP* **1305** (2013) 131, [arXiv:1210.8141 \[hep-ph\]](#).
- [26] Y.-F. Li, J. Cao, Y. Wang, and L. Zhan, “Unambiguous Determination of the Neutrino Mass Hierarchy Using Reactor Neutrinos,” [arXiv:1303.6733 \[hep-ex\]](#).
- [27] S. J. Parke, H. Minakata, H. Nunokawa, and R. Z. Funchal, “Mass Hierarchy via Mossbauer and Reactor Neutrinos,” *Nucl.Phys.Proc.Suppl.* **188** (2009) 115–117, [arXiv:0812.1879 \[hep-ph\]](#).
- [28] Y. Wang, “Daya Bay II: the next generation reactor neutrino experiment,” in *NuFACT 2012*. Jul, 2012.
- [29] Y. Wang, “Daya Bay II: current status and future plan,” in *Daya Bay II First Meeting*. Jan, 2013.
- [30] X. Qian, A. Tan, W. Wang, J. Ling, R. McKeown, *et al.*, “Statistical Evaluation of Experimental Determinations of Neutrino Mass Hierarchy,” *Phys.Rev.* **D86** (2012) 113011, [arXiv:1210.3651 \[hep-ph\]](#).
- [31] **IceCube** Collaboration, IceCube Collaboration, “PINGU Sensitivity to the Neutrino Mass Hierarchy,” [arXiv:1306.5846 \[astro-ph.IM\]](#).
- [32] Y. Wang, “JUNO: current status and future plan,” in *JUNO Meeting at IHEP, Beijing, China*. Jul, 2013.
- [33] Y.-K. Heng, “The central detector design and acrylic option.” Jul, 2013.
- [34] Y.-K. Heng, “The progress of the central detector.” Oct, 2013.
- [35] Y.-Y. Ding, “Liquid scintillator for JUNO,” in *JUNO Meeting at IHEP, Beijing, China*. Jul, 2013.

- [36] S. Qian, “The status of the MCP-PMT R&D,” in *JUNO Meeting at IHEP, Beijing, China*.
- [37] SNO Collaboration, J. Boger *et al.*, “The Sudbury neutrino observatory,” *Nucl.Instrum.Meth.* **A449** (2000) 172–207, [arXiv:nucl-ex/9910016](#) [[nucl-ex](#)].
- [38] KamLAND Collaboration, B. Berger *et al.*, “The KamLAND Full-Volume Calibration System,” *JINST* **4** (2009) P04017, [arXiv:0903.0441](#) [[physics.ins-det](#)].
- [39] Super-Kamiokande Collaboration, M. Nakahata *et al.*, “Calibration of Super-Kamiokande using an electron linac,” *Nucl.Instrum.Meth.* **A421** (1999) 113–129, [arXiv:hep-ex/9807027](#) [[hep-ex](#)].
- [40] Super-Kamiokande Collaboration, E. Blaufuss *et al.*, “N-16 as a calibration source for Super-Kamiokande,” *Nucl.Instrum.Meth.* **A458** (2001) 638–649, [arXiv:hep-ex/0005014](#) [[hep-ex](#)].
- [41] J. Liu, B. Cai, R. Carr, D. Dwyer, W. Gu, *et al.*, “Automated Calibration System for a High-Precision Measurement of Neutrino Mixing Angle θ_{13} with the Daya Bay Antineutrino Detectors,” [arXiv:1305.2248](#) [[physics.ins-det](#)].
- [42] M. Dragowsky, A. Hamer, Y. Chan, R. Deal, E. Earle, *et al.*, “The N-16 calibration source for the Sudbury Neutrino Observatory,” *Nucl.Instrum.Meth.* **A481** (2002) 284–296, [arXiv:nucl-ex/0109011](#) [[nucl-ex](#)].
- [43] N. Tagg, A. Hamer, B. Sur, E. Earle, R. Helmer, *et al.*, “The Li-8 calibration source for the Sudbury Neutrino Observatory,” *Nucl.Instrum.Meth.* **A489** (2002) 178–188, [arXiv:nucl-ex/0202024](#) [[nucl-ex](#)].
- [44] W. Bauer, “The Stuttgart Positron Beam, its Performance and Recent Experiments,” *Nucl.Instrum.Meth.* **B50** (1990) 300.
- [45] V. Shvedunov, “Low-Energy Electron Accelerator Applications”, <http://icc.ub.edu/congress/ESP-RUS2011/>.
- [46] C. Piel, *et al.* “A 0.5 to 50 MeV Electron Linear Accelerator System”, Particle Accelerator Conference (2007).
- [47] National Electrostatics Corporation (NEC) <http://www.pelletron.com/>.
- [48] NIHV Corporation, <http://www.nhv.jp/en/index.html>.
- [49] Research Instruments GmBH, <http://www.research-instruments.de/frontend/publications-linear-accelerators>.
- [50] H. Huang, X. Ruan, J. Ren, C. Fan, Y. Chen, *et al.*, “Manual Calibration System for Daya Bay Reactor Neutrino Experiment,” *JINST* **8** (2013) P09013, [arXiv:1305.2343](#) [[physics.ins-det](#)].